Molecular Mechanisms of Band 3 Inhibitors. 3. Translocation Inhibitors†

Joseph J. Falke‡ and Sunney I. Chan*

Arthur Amos Noyes Laboratory of Chemical Physics, California Institute of Technology, Pasadena, California 91125

Received February 13, 1986; Revised Manuscript Received July 7, 1986

ABSTRACT: During the translocation of the band 3 transport site between the inward- and outward-facing orientations, the Cl^- transport site complex passes through a transition state lying on the reaction pathway between the two extreme orientations. Niflumic acid, 2-[(7-nitrobenzofurazan-4-yl)amino]ethanesulfonate, and 2,4,6-trichlorobenzenesulfonate each are translocation blockers that can bind to both the inward- and outward-facing conformations of band 3. The principal mechanism of these inhibitors is a reduction in the translocation rate, since they have essentially no effect on (a) the apparent K_D for Cl^- binding to the transport site and (b) the migration of Cl^- between the transport site and solution. Instead, these inhibitors raise the free energy of formation of the transition state during translocation and thereby can lock the transport site into either the inward- or outward-facing orientation. In contrast, 2,4-dinitrofluorobenzene (DNFB) appears to restrict the accessibility of the transport site to solution Cl^-; also, the DNFB reaction rate is increased by Cl^-, suggesting that DNFB modification may occur during translocation. Thus DNFB is proposed to trap the Cl^-–transport site complex site during translocation to yield a conformation intermediate to the inward- and outward-facing orientations. A model is presented for the molecular mechanism of transport across biological membranes. The transport machinery is proposed to contain ≥6 transmembrane helices that surround a central channel containing a sliding hydrophobic barrier. The transport site lies between two of the channel-forming helices and remains stationary while the hydrophobic barrier slides from one end of the channel to the other, thereby exposing the transport site to the opposite solution compartment.

Transport proteins possess the molecular machinery necessary to expose bound substrate to the solution compartment on the opposite side of the membrane. The nature of this transport machinery is unknown, and molecules that interact with the machinery are potentially useful as probes of the transport event. Inhibitors that slow the transport event while leaving the transport site and substrate channels intact are termed translocation inhibitors. Such inhibitors can provide a variety of information: the details of the inhibitory reaction provide insight into the mechanism of the machinery, while the location of the inhibitory site pinpoints the transport machinery in the primary and higher-order structure of the protein.

In this study, we show that numerous inhibitors of band 3 catalyzed anion transport are translocation inhibitors and that these inhibitors can be categorized into two subsets. Successful completion of a transport event requires the passage of the substrate–transport site complex through a transition state in which the transport site is located between its inward- and outward-facing orientations: *translocation trappers* lock the site into an intermediate conformation, while *translocation blockers* lock the transport site into the extreme inward- or outward-facing orientations. Both types of inhibitors leave the transport site and substrate channels intact, indicating that the transport machinery includes protein domains that are structurally distinct from the anion binding domains. On the basis of the information presently available, a structural model for the transport machinery is developed that is consistent with the behavior of transport site inhibitors, channel blockers, and translocation inhibitors, as well as other known features of the band 3 system.

Materials and Methods

All experimental details are described under Materials and Methods in the first paper of three in this issue (Falke & Chan, 1986a).

Results

Strategy of Translocation Inhibitor Identification. ^{35}Cl NMR observations of Cl^- binding to the band 3 transport site can be used to resolve translocation trappers and blockers from each other and from other classes of band 3 inhibitors. When Cl^- binds with high affinity to a homogeneous class of sites, a characteristic square hyperbola is observed on a plot of $^{35}Cl^-$ line broadening vs. $[Cl^-]^{-1}$, as is the case for band 3 transport sites (Falke et al., 1984a,b):

$$\delta_i = \alpha_i \frac{[X_i]_T}{K_{Di}} \frac{[Cl^-]^{-1}}{[Cl^-]^{-1} + K_{Di}^{-1}} \quad (1)$$

Here δ_i is the line broadening due to site X_i, α_i is a constant characteristic of the site, and K_{Di} is the Cl^- dissociation constant of the site. When the exchange of Cl^- between a site and solution is sufficiently slow, α_i is directly related to the rate at which bound Cl^- leaves the site; specifically, $\alpha_i = k_{off}/\pi$. This dependence of the transport site line broadening on the exchange of Cl^- between the site and solution can be used to investigate the accessibility of the site to the medium.

The accessibility of the transport site is inhibited by translocation trappers, which are proposed to lock the Cl^-–transport site complex into an intermediate state between the inward- and outward-facing conformations so that Cl^- cannot leave the site. Such inhibitors reduce k_{off} and correspondingly inhibit the transport site line broadening: in the extreme case the line broadening is reduced to zero. The inhibition due to

† Contribution No. 7345. This research was supported by Grant GM 22432 from the National Institute of General Medical Sciences, U.S. Public Health Service.

* Author to whom correspondence should be addressed.

‡ National Science Foundation Predoctoral Fellow. Present address: Department of Biochemistry, University of California, Berkeley, CA 94720.

0006-2960/86/0425-7899$01.50/0

translocation state trappers can be resolved from that due to transport site inhibitors or channel blockers by examining the Cl^- dependence: transport site trapping by a translocation trapper is facilitated by the presence of Cl^- in the transport site because the frequency of empty site translocation is ≥4 orders of magnitude slower than the translocation of the Cl^-–loaded site [reviewed by Knauf (1979)]. As a result, the binding of such an inhibitor is an increasing function of $[Cl^-]$, while binding of transport site inhibitors is a decreasing function of $[Cl^-]$ and the binding of channel blockers is independent of $[Cl^-]$ (Falke & Chan, 1986a,b).

Unlike translocation trappers, translocation blockers leave the transport site fully exposed to the medium. Translocation blockers lock the transport site into the inward- or outward-facing conformation such that Cl^- migration between the site and solution, as well as Cl^- binding to the site, remains unaltered. In this case the square hyperbola observed for the transport site on a plot of line broadening vs. $[Cl^-]^{-1}$ remains intact (eq 1). It is important to note that in principle the α_i and K_{Di} of the inward- and outward-facing orientations of the transport site can be different, and differences in K_{Di} can lead to deviations from a simple square hyperbola. However, a translocation blocker that recruits transport sites to one orientation will yield a homogeneous class of sites exhibiting a simple square hyperbola (eq 1). Similarly, a translocation blocker that allows the ping-pong mechanism to control the distribution of transport sites between the inward- and outward-facing orientations yields an apparently homogeneous class of sites exhibiting a simple square hyperbola: in this case the observed α_i and K_{Di} are weighted averages of the corresponding microscopic values (Falke & Chan, 1985). Thus, in the event that an apparently homogeneous class of transport sites is observed in the presence of inhibitor, the sidedness of the sites with respect to the membrane should be determined. An inhibitor that recruits sites will yield transport sites on only one side of the membrane, while an inhibitor that has no effect on the ping-pong distribution of sites will leave sites on both sides of the membrane (Falke et al., 1984b).

The following investigation of band 3 inhibitors suggests that 2,4-dinitrofluorobenzene is a translocation trapper, while niflumic acid, NBD-taurine,[1] and 2,4,6-trichlorobenzenesulfonate are shown to be translocation blockers.

2,4-Dinitrofluorobenzene (DNFB). The inhibition of anion transport by DNFB has been shown to stem from the dinitrophenylation of a single lysine residue on the 17-kDa chymotryptic/tryptic fragment of band 3. This lysine is also modified by 4,4′-diisothiocyanodihydrostilbene-2,2′-disulfonate (H_2DIDS) (Jennings & Passow, 1978; Shami et al., 1978). The rate of the inhibitory DNFB modification of band 3 is increased by increasing $[Cl^-]$ (Passow et al., 1980a,b), suggesting that the lysine modified by DNFB is not a transport site residue because a transport site residue would be protected by substrate. Instead, DNFB could be a transition state trapper which would be predicted to restrict the accessibility of the transport site to the medium, thereby inhibiting the transport site line broadening.

DNFB inhibits approximately 80% of the transport site line broadening (Figure 1). As previously observed in studies of anion transport inhibition by DNFB, the inhibition is less than complete: the competing reaction of DNFB with a lysine residue on the 35-kDa chymotryptic fragment is known to reduce the dinitrophenylation of the inhibitory site on the 17-kDa fragment (Rudolff et al., 1983). Thus the simplest

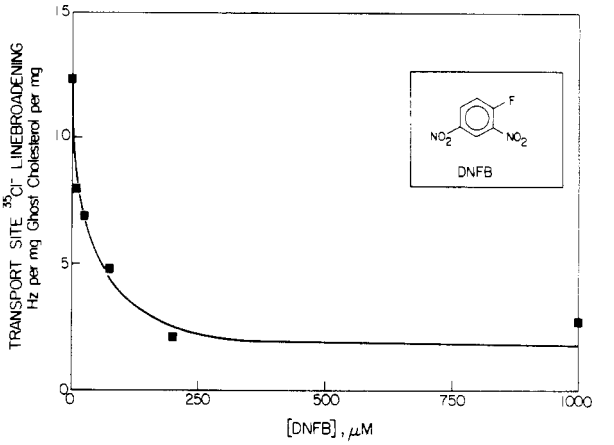

FIGURE 1: 2,4-Dinitrofluorobenzene inhibits transport site $^{35}Cl^-$ line broadening. Shown is the line broadening due to both inward- and outward-facing transport sites of leaky ghosts modified at 37 °C for 0.5 h with the indicated [DNFB] in 10 mM NaH_2PO_4, pH to 7.4 with NaOH, and 50 mM NaCl. The membranes were then washed with 100 mM NH_4Cl and 5 mM NaH_2PO_4, pH to 8 with NaOH and NH_4OH, and sonicated. Finally, the membranes were diluted with buffer to yield final sample compositions: 150 mM NH_4Cl and 5 mM NaH_2PO_4, pH to 8.0 with NaOH and NH_4OH, in 20% D_2O. In addition, the final samples contained 50 mM sodium citrate, pH 8, or 300 mM $NaHCO_3$, pH 8. The difference between the line broadening of samples ± HCO_3^- is the transport site line broadening. Spectral parameters: 8.8 MHz, 3 °C.

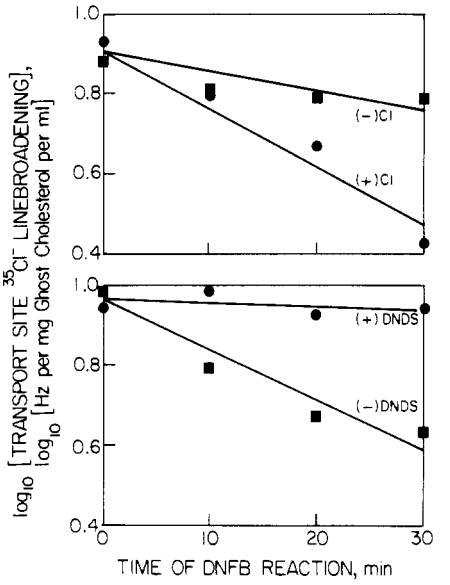

FIGURE 2: Effect of Cl^- and DNDS on the rate of DNFB inhibition of transport site $^{35}Cl^-$ line broadening. Shown is the line broadening due to both inward- and outward-facing transport sites on leaky ghosts labeled with DNFB in the presence or absence of Cl^- or DNDS. The solid lines are linear least-squares best-fit straight lines. Leaky ghosts were washed with 10 mM NaH_2PO_4 and 50 mM NaCl, pH to 7.4 with NaOH, and then diluted with buffer to yield 200 μM NaH_2PO_4, pH to 7.4 with NaOH, and 150 mM NaCl [(+)Cl^-]; 25 mM sodium citrate [(−)Cl^-]; 50 mM NaCl and 250 μM DNDS [(+)DNDS]; or 50 mM NaCl and no DNDS [(−)DNDS]. Following reaction at 37 °C for the indicated time, an aliquot was removed to ice, then washed in 100 mM NH_4Cl and 5 mM NaH_2PO_4, pH to 8 with NaOH and NH_4OH, and sonicated. Finally, the sample was diluted to yield the same final compositions described in Figure 1. Spectral parameters: 8.8 MHz, 3 °C.

[1] Abbreviations: DNFB, 2,4-dinitrofluorobenzene; NIF, niflumic acid; NBD-taurine or NBDT, 2-[(7-nitrobenzofurazan-4-yl)amino]ethanesulfonate; TCBS, 2,4,6-trichlorobenzenesulfonate; DNDS, 4,4′-dinitrostilbene-2,2′-disulfonate; SITS, 4-acetimido-4′-isothiocyanostilbene-2,2′-disulfonate; H_2DIDS, 4,4′-diisothiocyanodihydrostilbene-2,2′-disulfonate; NAP-taurine or NAPT, 2-[(4-azido-2-nitrophenyl)amino]-ethanesulfonate; PG, phenylglyoxal; pNBS, *p*-nitrobenzenesulfonate; ROV, sealed right-side-out vesicles.

Table I: Effect of Anions on the DNFB Reaction

anion	time of DNFB reaction at 37 °C (min)						
	0			30			
	δ^a			δ^a			
	0 mM DNDS	1 mM DNDS	Δ^b	0 mM DNDS	1 mM DNDS	Δ^b	protection (%)
(1) none[c]			7.6 ± 0.6			6.2 ± 0.0	
(2) 150 mM Cl^-[c]			8.5 ± 1.2			2.8 ± 0.8	−400 ± 100
(3) 50 mM Cl^-[c]	8.5 ± 0.1	5.5 ± 0.0	3.0	6.1 ± 0.0	4.8 ± 0.2	1.3	
(4) 50 mM Cl^-, 200 mM niflumic acid[c]	7.0 ± 0.2	4.9 ± 0.1	2.9	5.8 ± 0.1	3.9 ± 0.1	1.9	53 ± 17
(5) 50 mM Cl^-, 1 mM 2,4,6-trichlorobenzenesulfonate[c]	7.5 ± 0.2	4.6 ± 0.2	2.9	6.2 ± 0.1	4.4 ± 0.2	1.8	47 ± 24
(6) 50 mM Cl^-, 200 μM DNDS[c]	7.6 ± 0.2	4.7 ± 0.2	3.0	6.9 ± 0.2	4.7 ± 0.2	2.2	70 ± 26

[a] δ, transport site $^{35}Cl^-$ line broadening in Hz/(mg of membrane cholesterol/mL). [b] Δ, total $^{35}Cl^-$ line broadening in Hz/(mg total ghost protein/mL). [c] Leaky ghosts were washed with 10 mM NaH_2PO_4 and 50 mM NaCl, pH to 7.4 with NaOH, and then diluted with buffer to yield 200 μM NaH_2PO_4 and 1 mM NaCl, pH to 7.4 with NaOH, plus (rows 1 and 2) 25 mM sodium citrate or 150 mM NaCl or (rows 3–6) 50 mM Cl^- and the indicated additional inhibitor. Following reaction at 37 °C for the indicated time, an aliquot was removed to ice and then washed in 100 mM NH_4Cl and 5 mM NaH_2PO_4, pH to 8 with NaOH and NH_4OH, and sonicated. Finally, the sample was diluted to yield the final sample composition: 150 mM NH_4Cl, 20% D_2O, and 5 mM NaH_2PO_4, pH to 8.0 with NH_4OH and NaOH, and (rows 1 and 2) 50 mM sodium citrate or 300 mM $NaHCO_3$, pH 8, (rows 3–6) 0 or 1 mM DNDS. Spectral parameters: 8.8 MHz, 3 °C. The indicated protection values are relative to the reaction $[Cl^-]$ values of (rows 1 and 2) 1 or (rows 3–6) 50 mM.

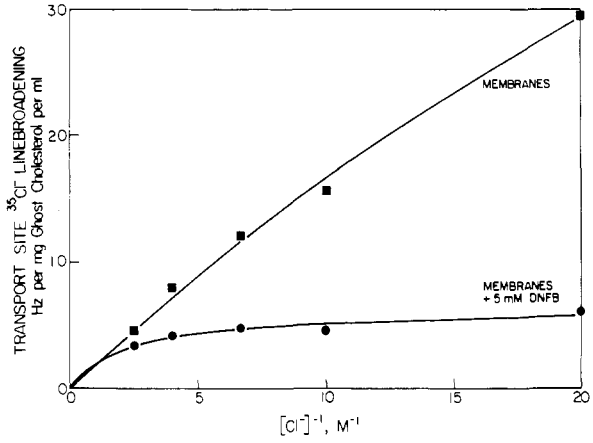

FIGURE 3: $[Cl^-]$ dependence of transport site $^{35}Cl^-$ line broadening due to DNFB-modified membranes. Shown is the line broadening due to transport sites on leaky ghost membranes ± DNFB modification. The solid curves are nonlinear least-squares best-fit curves for a set of modified membranes [lower curve, $y = Ax/(K_D x + 1)$, K_D = 460 ± 80 mM] and a set of unmodified membranes (upper curve, K_D = 20 ± 10 mM). Leaky ghost membranes were modified with 800 μM DNFB at 37 °C for 0.5 h and then washed and sonicated as described in Figure 1. Finally, the membranes were diluted with buffer to yield the indicated $[NH_4Cl]$ and 2.5 mM NaH_2PO_4 in 20% D_2O, pH to 8 with NaOH and NH_4OH. Sufficient citric acid, pH to 8 with NaOH, was added to bring the ionic strength up to that of the $[NH_4Cl]$ = 400 mM sample. Spectral parameters: 8.8 MHz, 3 °C.

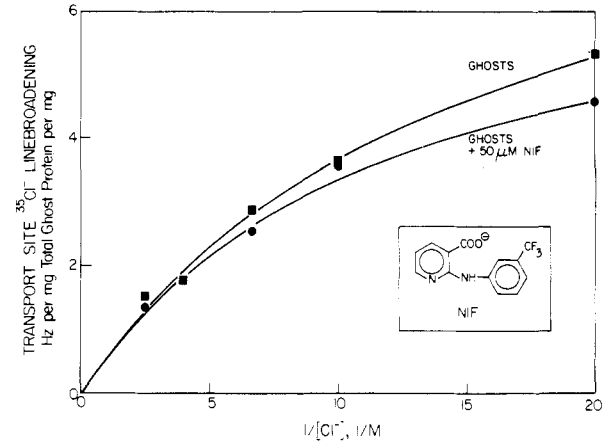

FIGURE 4: Niflumic acid leaves transport site $^{35}Cl^-$ line broadening intact. Shown is the line broadening due to both inward- and outward-facing transport sites on leaky ghosts in the absence or presence of 50 μM NIF. The solid curves are nonlinear least-squares best-fit curves [$y = Ax/(K_D x + 1)$, K_D = 60 ± 10 mM or 80 ± 10 mM in the absence or presence of NIF, respectively]. Final buffer composition is as in Figure 3. Spectral parameters: 8.8 MHz, 3 °C.

explanation of the transport site line broadening inhibition by DNFB is that the bulk of the observed line broadening inhibition occurs when 80% of the transporters are modified in the 17-kDa region in a reaction that exhibits a DNFB titration curve (Figure 1) and a rate enhancement by Cl^- (Figure 2 and Table I) that are the same, within error, as those previously observed for modification at this site (Rudloff et al., 1983). The remaining 20% of the transporters are modified in the 35-kDa region, and modification at this second site reduces the affinity of the transport site for Cl^- but does not completely eliminate the line broadening due to the transport site [K_D = 80 ± 20 mM before DNFB (Falke et al., 1984a), K_D = 460 ± 80 mM after DNFB (Figure 3)].

If DNFB traps the transport site during a translocation, then inhibitors that block the translocation should protect band 3 against inhibition by DNFB. The inhibitor DNDS, which recruits transport sites to the outward-facing conformation and thereby inhibits translocation [reviewed by Macara and Cantley (1983) and Falke et al. (1984a, 1986a)], significantly slows the rate of line broadening inhibition by DNFB (Figure 2 and Table I). Similarly niflumic acid (NIF) and 2,4,6-trichlorobenzenesulfonate (TCBS) slow the rate of line broadening inhibition by DNFB (Table I). These results are completely consistent with a model in which DNFB traps the transport site during translocation, since NIF and TCBS are shown by the following results to be translocation blockers.

Niflumic Acid (NIF). The anionic form of NIF is known to bind to an extracellular site on band 3 and thereby inhibit anion transport. The NIF binding site overlaps the binding site of the stilbenedisulfonate class of transport site inhibitors, since the binding of NIF and that of 4-acetimido-4′-isothiocyanostilbene-2,2′-disulfonate (SITS) are mutually exclusive. However, NIF does not bind to the transport site itself since NIF does not compete with Cl^- for binding. It has thus been proposed that NIF binds to a site distinct from the transport site and inhibits anion transport by blocking translocation (Cousin & Matais, 1979; Knauf & Mann, 1984). This idea can be tested by ^{35}Cl NMR.

NIF has no effect on the transport site $^{35}Cl^-$ line broadening (Figure 4). This negative result is not due to loss of the NIF binding site, since NIF competes with DNDS (Figure 5, Table II) and pNBS (Table II), thereby dramatically restoring the

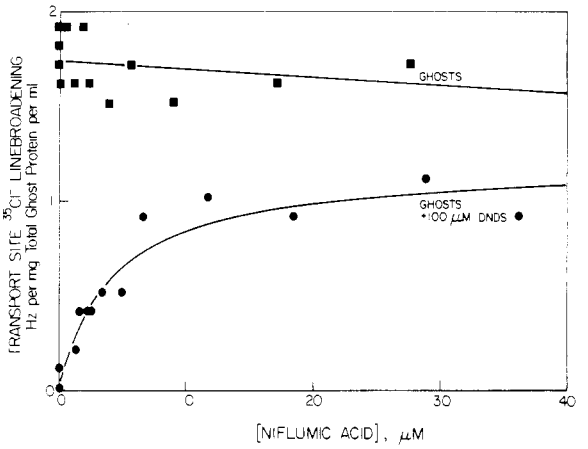

FIGURE 5: Niflumic acid restores transport site $^{35}Cl^-$ line broadening inhibited by DNDS. Shown is the line broadening due to both inward- and outward-facing transport sites on leaky ghost membranes. The data for membranes in the absence of DNDS are best fit by a nonlinear least-squares straight line (upper curve), while the data for membranes in the presence of DNDS are best fit by a nonlinear least-squares curve [lower curve, $y = Ax/(x + K_D)$, $K_D = 4 \pm 1$ μM]. Each sample contained the indicated [NIF] as well as 250 mM NH_4Cl and 2.5 mM NaH_2PO_4, pH to 8.0 with NH_4OH and NaOH, in 20% D_2O. Spectral parameters: 8.8 MHz, 3 °C.

Table II: Competition of NIF with DNDS and pNBS

	total $^{35}Cl^-$ line broadening [Hz/(mg of total ghost protein/mL)][a]	transport site inhibition (%)
ghosts	5.2 ± 0.2	
+50 μM NIF	5.2 ± 0.2	0
+100 μM DNDS	3.6 ± 0.2	100
+NIF + DNDS	4.6 ± 0.2	62
+7.5 mM pNBS	3.6 ± 0.0	100
+pNBS + NIF	4.5 ± 0.0	56

[a] Sample preparation and analysis as described in the legend to Figure 4.

transport site line broadening. The observation that NIF binding leaves the transport site line broadening intact indicates that (a) the pathway for diffusion of Cl^- between the transport site and solution remains open and (b) the transport site retains its native affinity for Cl^- (Figure 4). Thus inhibition of anion transport by NIF does not involve blocking of a substrate channel nor inhibition of Cl^- binding to the transport site. Instead, it follows that NIF is a translocation blocker that slows the movement of the substrate–transport site complex between the inward- and outward-facing orientations.

There are two potential mechanisms by which NIF could block translocation. NIF could recruit the transport site to the inward- or outward-facing conformation by stabilizing the free energy of one conformation relative to that of the other. Alternatively, NIF could increase the free energy of formation of the rate-limiting transition state during the translocation event; in this case, the opposing translocation rates would be slowed by the same factor, and the distribution of transport sites between the inward- and outward-facing conformations would remain unchanged (Gunn & Fröhlich, 1979; Falke & Chan, 1985). The ^{35}Cl NMR technique can be used to test for a change in the distribution of transport sites across the membrane (Falke et al., 1984a).

The ability of ^{35}Cl NMR to resolve inward- from outward-facing transport sites stems from the requirement that the bulk Cl^- population must sample a Cl^- binding site sufficiently rapidly on the NMR time scale or that site will not contribute to the line broadening of the bulk Cl^- resonance.

Table III: Effect of NIF on the Transmembrane Distribution of Transport Sites

	total $^{35}Cl^-$ line broadening[a]	transport site inhibition[b] (%)
cells	2.1 ± 0.1[c]	
+100 μM NIF	2.1 ± 0.1[c]	0
+100 μM DNDS	1.1 ± 0.1[c]	100
+DNDS + NIF	1.5 ± 0.1[c]	60
ROV	3.5 ± 0.1[d]	
+50 μM NIF	3.4 ± 0.1[d]	7
+1 mM DNDS	2.1 ± 0.1[d]	100
crushed ghosts	3.2 ± 0.1[d]	
+50 μM NIF	3.3 ± 0.1[d]	−9
+1 mM DNDS	2.1 ± 0.1[d]	100
sonicated ghosts	6.0 ± 0.2[d]	
+50 μM NIF	5.7 ± 0.2[d]	16
+1 mM DNDS	4.1 ± 0.1[d]	100

[a] Sample preparation and analysis as described under Materials and Methods. [b] Fraction inhibited = $(A - x)/(A - B)$, where A = line broadening of sample without inhibitor and B = linebroadening of sample with DNDS. [c] Values in units of 10^{-9} Hz/(cells/mL). [d] Values in units of Hz/(mg of total ghost protein/mL).

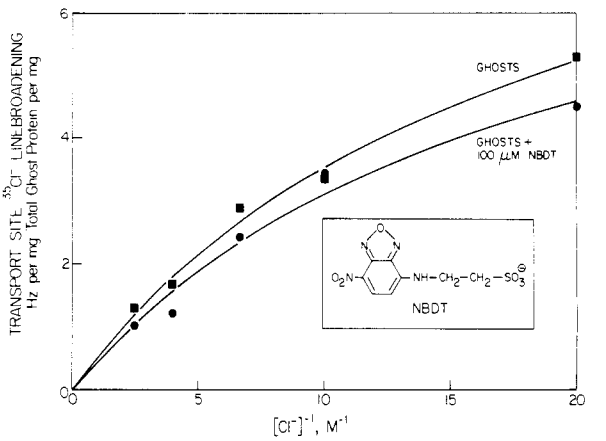

FIGURE 6: NBD-taurine leaves transport site $^{35}Cl^-$ line broadening intact. Shown is the line broadening due to both inward- and outward-facing transport sites on leaky ghosts in the absence or presence of 100 μM NBDT. The solid curves are nonlinear least-squares best-fit curves [$y = Ax/(K_D x + 1)$, $K_D = 50 \pm 10$ mM or 50 ± 10 mM in the absence or presence of NBDT, respectively]. Final buffer composition is as in Figure 3. Spectral parameters: 8.8 MHz, 3 °C.

In a sealed compartmentalized system such as the intact red cell, the bulk internal Cl^- population is invisible due to line broadening by the large hemoglobin population, so only the external bulk Cl^- is observed. In the sealed right-side-out vesicle (ROV) and crushed ghost systems, the bulk internal Cl^- population is too small to observe. Thus, in all three systems only the bulk external Cl^- population is observed, and the line broadening due to outward-facing sites can be specifically monitored. In contrast, the sonicated ghost and leaky ghost systems are uncompartmentalized systems in which a single bulk Cl^- population extends throughout the entire volume and rapidly samples all membrane surfaces during the NMR time scale. Thus, in these two systems both inward- and outward-facing sites contribute to the observed line broadening. Finally, when the line broadening due to the outward-facing sites has been determined by using the former three systems and the line broadening due to both inward- and outward-facing sites has been measured by using the latter two systems, the line broadening due to inward-facing sites can be estimated by subtraction (Falke et al., 1984a).

Examination of the effect of NIF on the distribution of the transport site line broadening across the membranes of intact red cells, ROV, crushed ghosts, sonicated ghosts, and leaky

Table IV: Effect of NBDT and TCBS on the Transmembrane Distribution of Sites

	total $^{35}Cl^-$ line broadening[a]	transport site inhibition[b] (%)
cells	1.4 ± 0.2[c]	
+100 μM NBDT	1.3 ± 0.2[c]	11
+10 mM NBDT	0.3 ± 0.1[c]	120
+100 μM DNDS	0.5 ± 0.1[c]	111
crushed ghosts	3.7 ● 0.0[d]	
+47 μM NBDT	3.7 ● 0.1[d]	0
+460 μM TCBS	3.4 ± 0.2[d]	21
+500 μM DNDS	2.3 ± 0.1[d]	100
ghosts	6.6 ± 0.0[d]	
+47 μM NBDT	6.8 ± 0.1[d]	−10
+460 μM TCBS	6.0 ± 0.0[d]	27
+500 μM DNDS	4.4 ± 0.1[d]	100

[a] Sample preparation and analysis as described under Materials and Methods. [b] Fraction inhibited = $(A - x)/(A - B)$, where A = line broadening of sample without inhibition and B = line broadening of sample with DNDS. [c] Values in units of 10^{-9} Hz/(cell/mL). [d] Values in units of Hz/(mg of total ghost protein/mL).

ghosts indicates that NIF has little effect on this distribution. Essentially no increase or decrease is observed for the line broadening due to outward-facing sites (intact cells, ROV, crushed ghosts; Table III), and similarly, essentially no change is observed for the line broadening due to both inward- and outward-facing sites (sonicated ghosts; Table III). The simplest interpretation of these data is that under the equilibrium conditions employed here NIF binds with nearly the same affinity to the inward- and outward-facing conformation of band 3 (affinities differ by a factor of ≤1.3), so that NIF leaves the distribution of transport sites essentially unchanged.[2]

Regardless of interpretation, the data of Table III demonstrate that NIF binds to both the inward- and outward-facing orientations of the transport site and slows both the in–out and out–in translocations. As a result, the distribution of sites between the inward- and outward-facing orientations remains under the control of the ping-pong mechanism, which is known to yield an apparently homogeneous population of sites (Falke & Chan, 1985; also Figure 4). Thus NIF is a translocation blocker that can lock the transport site into either the inward- or outward-facing orientation.

NBD-taurine (NBDT). The behavior of NBDT is similar to that of NIF in many respects. The monoanion NBDT binds

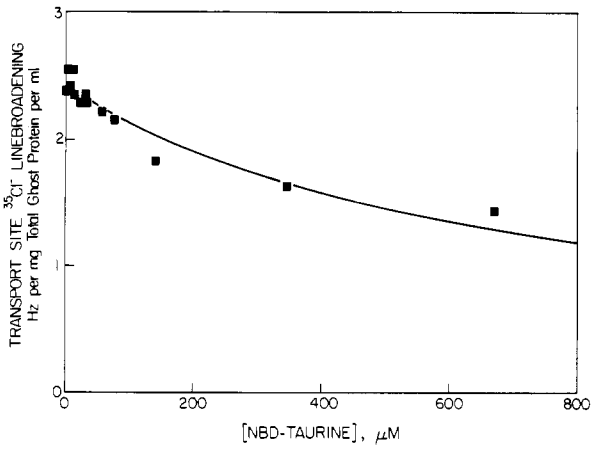

FIGURE 7: Effect of high [NBD-taurine] on transport site $^{35}Cl^-$ line broadening. Shown is the line broadening due to both inward- and outward-facing transport sites on leaky ghosts. The solid curve is a nonlinear least-squares best-fit curve for a set of homogeneous NBDT binding sites [$y = A[1 - x/(x + K_D)]$, $K_D = 750 \pm 50$ μM]. Samples contained 200 mM NH_4Cl and 5 mM NaH_2PO_4, pH to 8 with NH_4OH and NaOH, in 17.5% D_2O. Spectral parameters: 8.8 MHz, 3 °C.

to an extracellular inhibitory site on band 3 with high affinity ($K_D = 7.3 \pm 1.4$ μM at $[Cl^-] = 0$ mM) (Eidlemann et al., 1981). Cl^- competes with NBDT binding to this site; however, the affinity of Cl^- for the site is lower than that of Cl^- binding to the transport site (Eidlemann et al., 1981); thus the high-affinity binding of NBDT is not at the transport site. At sufficiently high concentrations, however, NBDT is known to bind with low affinity to the inward-facing transport site ($K_D = 3.5 \pm 1.5$ mM at $[Cl^-] = 0$ mM) (Eidlemann et al., 1981). Structurally, NBDT is similar to NAP-taurine (NAPT), which may have a similar inhibitory mechanism.

Like NIF, a concentration of NBDT (100 μM) sufficient to nearly saturate the high-affinity inhibitory sites ($K_D = 15$ μM at $[Cl^-] = 200$ mM) (Eidlemann et al., 1981) has no effect on the transport site line broadening (Figure 6). Thus NBDT leaves the transport site and the substrate channels leading to the transport site intact, while slowing the translocation of the transport site across the membrane. Examination of the distribution of transport site line broadening across the membranes of intact cells, crushed ghosts, and leaky ghosts indicates that NBDT binding to the high-affinity inhibitory site alters the distribution by a factor of ≤1.3 (Table IV). Thus NBDT binds to both the inward- and outward-facing conformations of band 3 and slows both the in–out and out–in translocations, so that the distribution of sites remains under the control of the ping-pong mechanism, which gives rise to an apparently homogeneous class of sites [Figure 6; also Falke & Chan (1985)]. It follows that NBDT, like NIF, is a translocation blocker that can lock the transport site into either the inward- or outward-facing orientation. At higher concentrations, NBDT begins to inhibit the transport site line broadening by binding to a site with an apparent dissociation constant of 750 ± 60 μM (at $[Cl^-] = 200$ mM, Figure 7). This site is neither the high-affinity inhibitory site ($K_D = 15$ μM at $[Cl^-] = 200$ mM) nor the inward-facing transport site ($K_D = 6$ mM at $[Cl^-] = 200$ mM) (Eidlemann et al., 1981), suggesting that it may be the outward-facing transport site.

2,4,6-Trichlorobenzenesulfonate (TCBS). The monoanion TCBS might be predicted to inhibit the transport site, as do DNDS and *p*-nitrobenzenesulfonate [reviewed by Knauf (1979)]. However, like NIF and NBDT, TCBS leaves the transport site line broadening intact and does not significantly alter the transmembrane distribution of sites (Table IV). Thus

[2] Under conditions that generate a $[Cl^-]$ gradient across the membrane, NIF is known to bind with considerably higher affinity to the outward-facing conformation of band 3 [affinities differ by a factor of 4–5 (Knauf & Mann, 1984; also P. Knauf, personal communication)]. Thus an alternative interpretation of the data of Table III is that NIF shifts the distribution of transport sites toward the outward-facing conformation and concomitantly increases the K_D for Cl^- binding to the outward-facing transport site so that the amount of outward-facing Cl^- transport site complex remains unchanged. Such an interpretation must also predict that NIF concomitantly decreases the K_D for Cl^- binding to the inward-facing transport site so that the amount of inward-facing Cl^- transport site complex remains unchanged (P. Knauf, personal communication). In this way, compensatory changes in the K_D for Cl^- binding could yield the observed properties of this system: (1) the distribution of transport site line broadening across the membrane would be essentially unchanged by NIF (Table III) because the concentration of the Cl^- transport site complex on the two sides of the membrane would remain unchanged; (2) the apparent K_D for Cl^- binding to transport sites would be essentially unchanged by NIF (Figure 3) because this apparent K_D would be a weighted average of the microscopic K_D's of the inward- and outward-facing transport sites (Falke & Chan, 1985); and (3) the apparent K_D for NIF binding to band 3 would be relatively independent of Cl^- (Cousin & Motais, 1979) because this apparent K_D would be a weighted average of the microscopic K_D's of the inward- and outward-facing conformations.

NIF, NBDT, and TCBS all belong to the translocation blocker class: these molecules leave the transport site and substrate channel intact, but they increase the activation free energy of the rate-limiting transition state during translocation.

The results summarized here indicate that NIF, NBDT, and TCBS each interact with the translocation machinery and may be useful for locking the transport site into either the inward- or outward-facing orientation, while DNFB may be useful in the stabilization of the translocation machinery during the transport event.

Discussion

An adequate model for the anion transport machinery of band 3 must explain a wide range of experimental observations: the transport site consists of one or a few positive charges buried within the membrane where it is inaccessible to proteases (Falke et al., 1985b). This buried site is alternatively exposed to the solution compartment on opposite sides of the membrane during the ping-pong transport cycle [reviewed by Macara and Cantley (1983), Falke et al. (1984b), and Falke and Chan (1985)], and the site can only cross the membrane when occupied by a monovalent anion [reviewed by Knauf (1979)]. The transport machinery can translocate both small substrates such as Cl^- and large substrates such as *p*-aminobenzenesulfonate (Aubert & Motais, 1975; Knauf, 1979). The transport process can be inhibited by three types of molecules which (1) occupy the transport site, (2) do not occupy the site but block a channel leading from the site to the solution, or (3) do not occupy the site but interfere with translocation of the site. The translocation of bound anion exhibits a large temperature (20–30 kcal/mol for Cl^-; Brahm, 1977) and pressure (Canfield & Macey, 1984) dependence and is rapid at physiological temperatures (turnover rate for Cl^- self-exchange is $>5 \times 10^4$/s at 37 °C; Brahm, 1977). The rate-limiting step in the Cl^- transport cycle is the translocation of bound Cl^- since the exchange of Cl^- between the site and solution is significantly faster than the turnover rate at both 3 and 37 °C (Falke et al., 1985a). This rapid migration of Cl^- between the site and solution suggests the presence of positive charges in the channel leading to the site. Finally, at least seven membrane-spanning segments have been chemically confirmed in the single polypeptide chain of the band 3 monomer (Jennings et al., 1984; Jennings & Nicknish, 1984), and the primary sequence of mouse band 3 is consistent with at least 12 membrane-spanning α-helices (Kopito & Lodish, 1985).

The hydrophobic barrier model (Figure 8) successfully explains many features of band 3 catalyzed anion transport. This model proposes that the 55-kDa transport domain, produced by tryptic or chymotryptic removal of the 40-kDa soluble N-terminal fragment (Steck et al., 1976; Jenkins & Tanner, 1977), consists of a channel surrounded by six or more membrane-spanning α-helical rods that are tightly associated within the membrane (Figure 8). Outside of the channel near its mouth are positive charges that increase the activity of anions in the vicinity of the channel: these charges are suggested to be among the low-affinity chloride binding sites observed by ^{35}Cl NMR (Falke et al., 1984b). Inside the channel are (1) one or more positive charges that facilitate anion movement through the channel, (2) a transport site that is composed of a single positively charged arginine residue lying in a hydrophobic cleft between two transmembrane helices, and (3) a hydrophobic barrier that consists of a helical hydrophobic region flanked by two random coil regions. Initially, the hydrophobic barrier cannot migrate past the charged site, but neutralization of the site by a monovalent anion allows

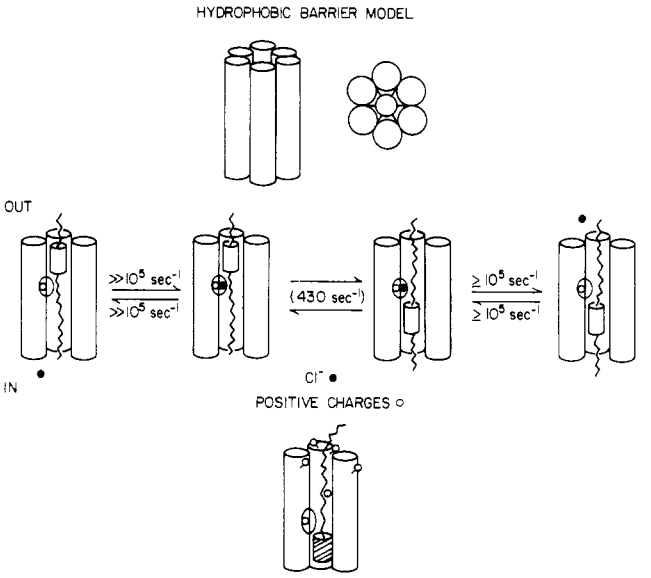

FIGURE 8: The sliding barrier model. Shown is a schematic representation of the band 3 monomer. The channel-forming α-helices (>6 helices) surround a hydrophobic barrier helix. The ion translocation event occurs when substrate anion neutralizes the charge in the transport site so that the hydrophobic barrier can slide past the site. Also shown are (1) positive charges near the mouth of the channel that increase the activity of anions in the vicinity of the channel, (2) positive charges within the channel that facilitate migration of anion within the channel, and (3) a single positively charged arginine residue in the transport site. The indicated rates are events per transport site per second at 0–3 °C. (Falke et al., 1985a; Fröhlich & Gunn, 1981).

barrier migration to occur so that the site becomes newly exposed to the opposite solution. This rate-determining barrier migration step accounts for (1) the rapid turnover rate, since the conformational change is on a small scale, (2) the observed transport of large organo anions, since these molecules could intercalate into the transport site cleft where they would not prevent barrier migration, and (3) the known discrepancy between the transport rates of divalent anions [reviewed by Knauf (1979)], since neutralization of the single transport site arginine is a prerequisite for barrier migration.

The hydrophobic barrier model is also consistent with each known type of anion transport inhibition. Transport site inhibitors occupy the transport site and thereby eliminate the transport site $^{35}Cl^-$ line broadening (Falke & Chan, 1986a). These inhibitors—including the stilbene disulfonates—have been extensively studied: the required planarity of these molecules is consistent with the idea that the transport site to which they bind is intercalated between two transmembrane helices. For example, the covalently bound stilbenedisulfonate 4-benzamido-4′-isothiocyanostilbene-2,2′-disulfonate (BIDS) has been shown to have low mobility and to lie in a hydrophobic environment within the membrane (Macara & Cantley, 1983). When bound, a large transport site inhibitor like BIDS projects into the channel and sterically prevents full translocation of the barrier: the resulting incomplete translocation locks the inhibitor into the site and partially exposes the inhibitor to the opposite solution compartment (Figure 9A). Moreover, it is observed (Verkman et al., 1983) that the binding of a reversible DNDS analogue such as 4,4′-dibenzamidostilbene-2,2′-disulfonate (DBDS) begins with rapid binding to a low-affinity site (proposed to be binding to the transport site), followed by slow binding to a high-affinity site (proposed to be locking of the inhibitor into a place by barrier migration over the site). Such partial translocation between the outward- and inward-facing conformations has been observed for the fluorescent inhibitor 5-maleimidoeosin (Macara

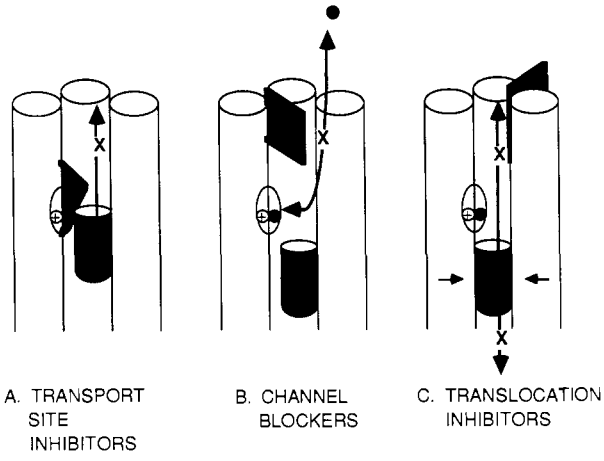

FIGURE 9: Inhibitors and the sliding barrier model. (A) A bound transport site inhibitor occupies the transport site and projects into the channel so that the barrier can slide partially over the inhibitor and lock it into place, as shown. The inhibitor sterically prevents the barrier from completing its migration so that the inhibitor is not transported. (B) A channel-blocking inhibitor projects into the channel, thereby slowing the exchange of Cl^- between the transport site and solution. The sliding barrier prevents access to the site from the opposite solution compartment. (C) A translocation inhibitor binds between two of the channel-forming α-helices, thereby changing the packing of the helices and sterically slowing the migration of the barrier. The inhibitor can lock the barrier in either the inward- or outward-facing orientation, such that anion migration through the channel and binding to the transport site are unimpaired.

& Cantley, 1983). It should be noted that the successful partial translocation of such a large molecule strongly supports the idea that the occupied transport site does not itself move during the translocation event.

Channel-blocking inhibitors are proposed to occupy a site within the channel, thereby slowing the migration of substrate between the site and solution [Figure 9B; also Falke and Chan (1986b)]. In the simplest picture a single molecule of inhibitor binds to the channel such that the inhibitor blocks one mouth of the channel while the hydrophobic barrier blocks the other. As a result, the transport site line broadening due to both inward- and outward-facing sites is eliminated.

Translocation blockers are proposed to bind between two transmembrane helices, thereby altering the packing of the channel-forming helices, which in turn causes steric hindrance of barrier migration (Figure 9C). Simultaneously, the transport site and substrate channel are left intact and remain accessible to substrate anion so that the transport site line broadening is unaffected (see Results). Like the transport site inhibitors, the translocation inhibitors contain flat, conjugated ring systems suitable for intercalation between hydrophobic helices. The binding site of the inhibitor need not be close to the point at which barrier migration is hindered, since a change in the helix packing at the binding site will affect the helix packing throughout the channel. Thus the hydrophobic barrier model provides a straightforward explanation for allosteric effects in the band 3 system.

Other features of anion transport that are consistent with the hydrophobic barrier model include the large temperature and pressure dependence of the turnover rate. The activation enthalpy is approximately 30 kcal/mol for all substrates studied [reviewed by Lowe and Lambert (1983)], which is consistent with a mechanism in which the substrate remains stationary during the rate-limiting translocation event. Both the large activation enthalpy and pressure dependence (Canfield & Macey, 1984) can be explained by an increase in the migration rate of the hydrophobic barrier when the channel expands. As the channel is heated, or as the lateral pressure on the channel decreases, the channel-forming helices move farther apart, thereby reducing the molecular friction between the barrier and the channel. In contrast to the activation enthalpies, the transport rates of the different substrates vary widely over a range spanning 4 orders of magnitude [reviewed by Knauf (1979)]. These differences can be explained by steric interactions: if the bound substrate projects into the channel, or if substrate binding changes the packing of the channel-forming helices, the migration of the hydrophobic barrier would be slowed. Thus different substrates are proposed to yield significantly different steric effects upon binding.

The sliding barrier model could have widespread applicability, since such a model can explain transport in a variety of transport systems. Some of the characteristic features of the sliding barrier model may be generally important for ion transport proteins: it is proposed that these proteins generally possess (1) surface charges that increase substrate ion activity near the mouth of the substrate channel, (2) a substrate channel leading from the surface of the protein to the buried transport site so that simple diffusion is able to carry out part of the process of transmembrane translocation, (3) a transport site buried in the hydrophobic interior of the protein where the thermodynamic driving force for lessening of the transport site total charge is strong, and (4) a requirement for the neutralization of the transport site total charge by substrate binding that contributes to substrate specificity.

It is also proposed that sliding barriers could be a general feature of transport proteins. This proposal is consistent with the primary sequences of band 3, the glucose transporter, Na,K-ATPase, and Ca,Mg-ATPase (Kopito & Lodish, 1985; Mueckler et al., 1985; Shull et al., 1985; MacLennen et al., 1985), which all appear to contain a sufficient number of transmembrane α-helices to surround a central channel containing a sliding barrier.

Finally, transmembrane α-helices are common structural components in nearly all current models describing the structure of membrane proteins. It is proposed that membrane proteins typically have substrate and inhibitor binding sites lying between two adjacent helices; as a result, allosteric effects due to changes in helix packing are likely to be widespread in membrane protein systems.

These ideas must be tested by a variety of structural approaches in order to develop an accurate molecular picture describing transport across biological membranes.

Registry No. DNFB, 70-34-8; NIF, 4394-00-7; DNDS, 128-42-7; pNBS, 138-42-1; NBDT, 75472-45-6; TCBS, 104778-51-0; Cl^-, 16887-00-6.

REFERENCES

Aubert, L., & Motais, R. (1975) *J. Physiol. (London) 246*, 159–179.

Brahm, J. (1977) *J. Gen. Physiol. 70*, 283–306.

Canfield, V. A., & Macey, R. I. (1984) *Biochim. Biophys. Acta 778*, 379–384.

Cousin, J. L., & Motais, R. (1979) *J. Membr. Biol. 46*, 125–153.

Eidelmann, O., Zangvill, M., Razon, M., Ginsburg, H., & Cabantchik, Z. I. (1981) *Biochem. J. 195*, 503–513.

Falke, J. J., & Chan, S. I. (1985) *J. Biol. Chem. 260*, 9537–9544.

Falke, J. J., & Chan, S. I. (1986a) *Biochemistry* (first of three papers in this issue).

Falke, J. J., & Chan, S. I. (1986b) *Biochemistry* (second of three papers in this issue).

Falke, J. J., Pace, R. J., & Chan, S. I. (1984a) *J. Biol. Chem. 259*, 6481–6491.

Falke, J. J., Pace, R. J., & Chan, S. I. (1984b) *J. Biol. Chem. 259*, 6472–6480.
Falke, J. J., Kanes, K. J., & Chan, S. I. (1985a) *J. Biol. Chem. 260*, 9545–9551.
Falke, J. J., Kanes, K. J., & Chan, S. I. (1985b) *J. Biol. Chem. 260*, 13294–13303.
Frölich, O., & Gunn, R. B. (1981) *Adv. Physiol. Sci., Proc. Int. Congr., 28th, 1980 6*, 275–280.
Gunn, R. B., & Frölich, O. (1979) *J. Gen. Physiol. 74*, 351–374.
Jenkins, R. E., & Tanner, M. J. A. (1977) *Biochem. J. 161*, 139–147.
Jennings, M. L., & Passow, H. (1978) *Biochim. Biophys. Acta 508*, 357–363.
Jennings, M. L., & Nicknish, J. S. (1984) *Biochemistry 23*, 6432–6436.
Jennings, M. L., Adams-Lackey, M., & Denney, G. H. (1984) *J. Biol. Chem. 259*, 4652–4660.
Knauf, P. A. (1979) *Curr. Top. Membr. Transp. 12*, 249–363.
Knauf, P. A., & Mann, N. A. (1984) *J. Gen. Physiol. 83*, 703–725.
Knauf, P. A., Ship, S., Breuer, W., McCulloch, L., & Rothstein, A. (1978) *J. Gen. Physiol. 72*, 607–630.
Kopito, R. R., & Lodish, H. F. (1985) *Nature (London) 316*, 234–238.
Lowe, A. G., & Lambert, A. (1983) *Biochim. Biophys. Acta 694*, 353–374.
MacLennan, D. H., Brandl, C. J., Korczak, B., & Green, N. M. (1985) *Nature (London) 316*, 696–700.
Muechler, M., Caruso, C., Baldwin, S. A., Panico, M., Bleach, F., Morris, H. R., Allard, W. J., Lienbard, G. E., & Lodish, H. F. (1985) *Science (Washington, D.C.) 229*, 941–945.
Passow, H., Fasold, H., Gartner, M., Legrum, B., Ruffing, W., & Zaki, L. (1980a) *Ann. N.Y. Acad. Sci. 341*, 361–383.
Passow, H., Kampmann, L., Fasold, H., Jennings, M., & Lepke, S. (1980b) in *Membrane Transport in Erythrocytes* (Lassen, U. V., Ussing, H. H., & Wieth, J. O., Eds.) Alfred Benzon Symp., Vol. 14, pp 345–367, Munksgaard, Copenhagen.
Rudloff, V., Lepke, S., & Passow, H. (1983) *FEBS Lett. 163*, 14–21.
Shami, Y., Rothstein, A., & Knauf, P. A. (1978) *Biochim. Biophys. Acta 599*, 127–139.
Shull, G. E., Schwartz, A., & Lingrel, J. B. (1985) *Nature (London) 316*, 691–695.
Steck, T. L., Ramos, B., & Stapazon, E. (1976) *Biochemistry 15*, 1154–1161.
Verkman, A. S., Dix, J. A., & Solomon, A. K. (1983) *J. Gen. Physiol. 81*, 421–449.

Complete Amino Acid Sequence of NADPH–Cytochrome P-450 Reductase from Porcine Hepatic Microsomes†

Mitsuru Haniu,‡ Takashi Iyanagi,§ Philip Miller,‡ Terry D. Lee,‡ and John E. Shively*,‡

Division of Immunology, Beckman Research Institute of the City of Hope, Duarte, California 91010, and Division of Biochemistry, Institute of Basic Medical Sciences, The University of Tsukuba, Ibaraki 305, Japan

Received April 24, 1986; Revised Manuscript Received July 10, 1986

ABSTRACT: The complete amino acid sequence of porcine hepatic microsomal NADPH–cytochrome P-450 reductase has been determined by microsequence analysis on several sets of proteolytic fragments. Sequence studies were performed initially on a 20-kilodalton (kDa) fragment and then on 80-kDa fragment. The amino-terminal end of the mature protein was blocked with an acetyl group, followed by 676 amino acid residues. It has been revealed that the COOH-terminal 20-kDa fragment has been derived from original enzyme by cleavage at the Asn–Gly (residues 502–503) linkage by an unknown mechanism. An NADPH-protected cysteine residue is located at residue 565, near a region exhibiting high sequence homology with ferredoxin–$NADP^+$ reductase. The FMN and FAD binding regions are possibly located in the amino-terminal region and the middle part of the protein molecule, respectively, as suggested by Porter and Kasper [Porter, T. D., & Kasper, C. B. (1985) *Proc. Natl. Acad. Sci. U.S.A. 82*, 973–977]. When this sequence is compared with that of rat enzyme, 60 amino acid residues are substituted, probably due to species differences. However, total sequence homology between these enzymes is 90%. Hydropathy plot analysis reveals that two regions from residues 27–43 and from residues 523–544 exhibit a high degree of hydrophobicity, suggesting membrane binding or interaction with cytochrome P-450.

Hepatic microsomal NADPH–cytochrome P-450 reductase is a flavoprotein which participates in hydroxylation of various endogenous and foreign compounds (Williams, 1976). This enzyme contains one molecule each of FAD and FMN per subunit in the active form and has a molecular weight of 78 000 (Iyanagi & Mason, 1973; Yasukochi & Masters, 1976). The catalytic function of this enzyme is electron transport from NADPH to cytochrome P-450 or cytochrome b_5 via FAD and FMN in the microsomal systems (French & Coon, 1979; Enoch & Strittmatter, 1979). Furthermore, this enzyme independently donates an electron to anticancer quinone drugs such as adriamycin and produces a free radical form of the anthracycline molecule which causes cell damage by DNA or RNA breakages (Bachur et al., 1978; Berlin & Haseltine, 1981).

† This work was supported by National Institutes of Health Grants GM 34426-01 (M.H.) and HD 14900 (J.E.S.).
* Correspondence should be addressed to this author.
‡ Beckman Research Institute of the City of Hope.
§ The University of Tsukuba.

0006-2960/86/0425-7906$01.50/0